Soft Matter

ROYAL SOCIETY OF CHEMISTRY

COMMUNICATION

Cite this: *Soft Matter*, 2020, **16**, 5571

Received 10th April 2020,
Accepted 2nd June 2020

DOI: 10.1039/d0sm00640h

rsc.li/soft-matter-journal

Crack density in bloodstains†

Junhee Choi,[a] Wonjung Kim *[b] and Ho-Young Kim *[a]

We construct a theoretical framework to understand the crack density of bloodstains by modeling whole blood as a suspension of binary size colloid particles. Our analysis based upon theories of soft capillarity and porous flows explains the observed increase of the crack density with increase of blood viscosity and decrease of environmental humidity. The results have direct implications on forensic science and medical diagnosis.

Human blood carries personal health information, which can be exploited for disease diagnosis or forensic analysis. Obtaining biomedical or forensic information from human blood typically requires complicated processes including centrifugation, mixing with cell biomarkers, and blood culturing.[1,2] Recently, it was suggested that cracks in bloodstains can reveal personal identity[3,4] and the environmental conditions during dehydration.[5,6] The analysis of the cracks eliminates the need for complicated post processes using bloodstains, which has thus raised great hopes toward techniques for prompt forensic or biomedical analysis. In this regard, a great deal of effort has been devoted to the experimental observations of crack patterns in bloodstains,[7–11] leading to the analysis of the dependence of the crack density on the humidity,[5,6] contact angle,[12] size[3] and thickness of the droplet.[13]

Because human whole blood is a biological colloid suspension including various cells and other viscoelastic biomaterials, the crack formation in bloodstains can be understood based on the theoretical framework for common colloid suspensions.[14–19] For instance, the increase of the inter-crack spacing in blood cracks with the droplet thickness[13] was rationalized by the results for an aqueous colloidal silica suspension.[14] Nevertheless, the remarkable complexity of the colloid composition of the whole blood has challenged a complete understanding of crack formation in bloodstains.

Here, we propose a theoretical model to elucidate the physical parameters that determine the blood crack density by modeling human whole blood as a suspension of binary size colloid particles. Our experimental observations of the crack formation reveal that the bloodstain is covered by a skin consisting of the blood plasma dispersion, which plays a key role in the crack formation. We go beyond the previous work of Lee *et al.* (2004),[16] which analysed the crack density in a film of mono-sized colloidal dispersions, by considering the different roles of the binary size particles, *i.e.* large blood cells and small proteins, in the crack formation. The results will bring us one step closer not only to understanding the dehydration process of biological substances but also to developing techniques for prompt forensic or biomedical analysis.

Human blood is a colloidal dispersion consisting of blood cells and plasma with each taking a volume fraction of approximately 50%. Among various kinds of blood cells such as red blood cells (RBCs), white blood cells and platelets, RBCs occupy approximately 90% of the entire cell volume. RBCs are an oval biconcave disk with a diameter of approximately 8 μm. Plasma contains water, proteins, and other substances such as minerals and lipids, and the volume fractions of water and proteins in plasma are 90% and 8%, respectively. The length of blood proteins greatly varies,[20] but albumin, a main constituent of blood proteins, is formed from long-string chains cross-linked with each other, whose single aggregation is assumed as a colloid particle with a size on the order of 10 nm.[21–24]

Fig. 1a displays the crack formation of a human whole blood droplet. The blood treated with an anticoagulant (K2EDTA)[4] was obtained from Seoul National University Hospital. The number of RBCs and the protein concentration were measured to be 5.2×10^6 mm^{-3} and 7 mg mm^{-3}, respectively, which were in the normal range. Additional haematological data are available in Table S1 (ESI†). A 5 μl blood droplet was placed on a bare glass slide in a thermo-hygrostat, where the temperature and relative humidity were kept at 20 °C and 40%, respectively. The water

[a] *Department of Mechanical Engineering, Seoul National University, Seoul 08826, Republic of Korea. E-mail: hyk@snu.ac.kr*
[b] *Department of Mechanical Engineering, Sogang University, Seoul 04107, Republic of Korea. E-mail: wonjungkim@sogang.ac.kr*

† Electronic supplementary information (ESI) available. See DOI: 10.1039/d0sm00640h

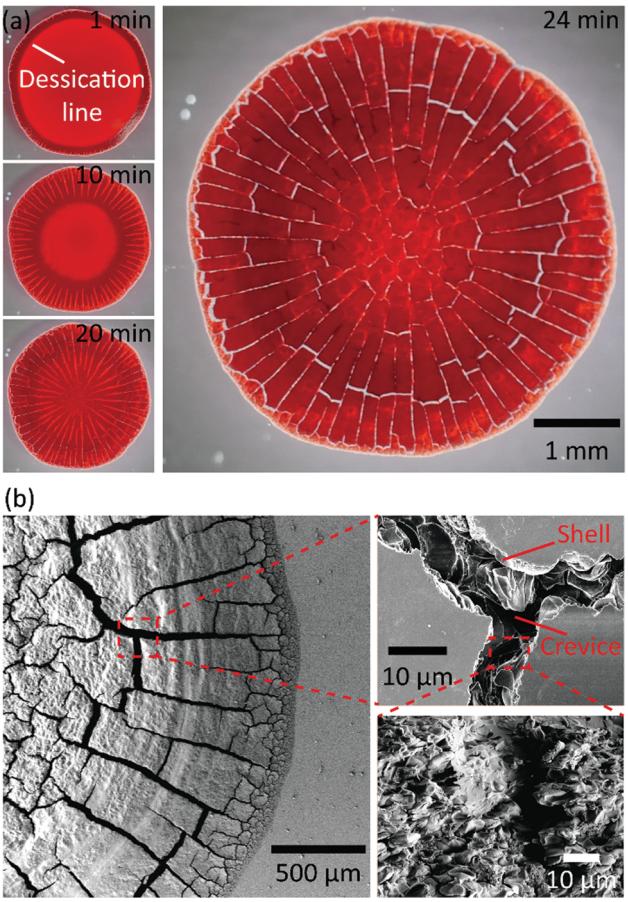

Fig. 1 Cracks of bloodstains. (a) Sequential images of crack formation of a blood droplet on a glass slide. The stain is thicker near the periphery, resembling a donut, although not evident in the two-dimensional optical microscope image. (b) SEM images of the cracks of a bloodstain. The right upper image displays the top view of the crevice, and the right lower image displays the interior surface seen through the crevice.

evaporation from the blood droplet caused a phase change from liquid to solid state, and a desiccation line was formed at the interface between the inner fluid and outer solidifying regions along the droplet perimeter within 1 min. As the solidifying region grew inwards, cracks began to appear behind the desiccation line and propagated inwards from the edge. The cracks were developed radially and thus orthogonal to the desiccation line. After 24 min, the cracks stopped growing.

Fig. 1b presents the scanning electron microscopy (SEM) images of the blood cracks. A shell structure covering the RBC grains was observed. We found that the cracks observed with the naked eye corresponded to the crevices on the shell. The interior surface seen through the crack was fairly bumpy owing to the RBC grains, and thus clearly distinct from the smooth shell surface. Given the proportion and shape of the constituents of the whole blood, we inferred that the shell was mainly composed of proteins, allowing us to envision the role of the proteins in the crack formation.

We start the theoretical analysis with a brief review of the process of crack formation in a droplet of a mono size colloid suspension.[16] When a colloid suspension drop is dehydrated, the solvent exclusively evaporates, leading to a rise of the colloid density. While the water–air–substrate contact line is pinned due to the aggregation of the colloid particles therein, a consolidated region grows inward from the contact line, where the closely packed particles create a porous structure.[25,26] Further evaporation yields concave menisci between the colloid particles, and the liquid–gas interface eventually retracts into the porous structure. Accordingly, the pressure inside the porous structure becomes lower than the atmosphere by the Laplace pressure, up to a maximum of $P_L \sim \sigma/r$ with σ the liquid–gas surface tension and r the colloid particle radius.[16,27,28] The magnitude of the Laplace pressure can be sufficiently large to cause a shrinkage of the elastic structure constructed by the closely packed particles. Meanwhile, the deformation can be limited on the bottom where the colloid particles stick to the surface due to the friction and adhesion forces. The strain difference in the thickness direction brings about tensile stresses on the top part of the porous structure. When the tensile stress is greater than the yield strength of the porous structure, cracking occurs, and the stored elastic energy is released through the rearrangement of the particle packing.[29,30]

We now turn to the crack formation of human whole blood. The above-mentioned experimental observations lead us to

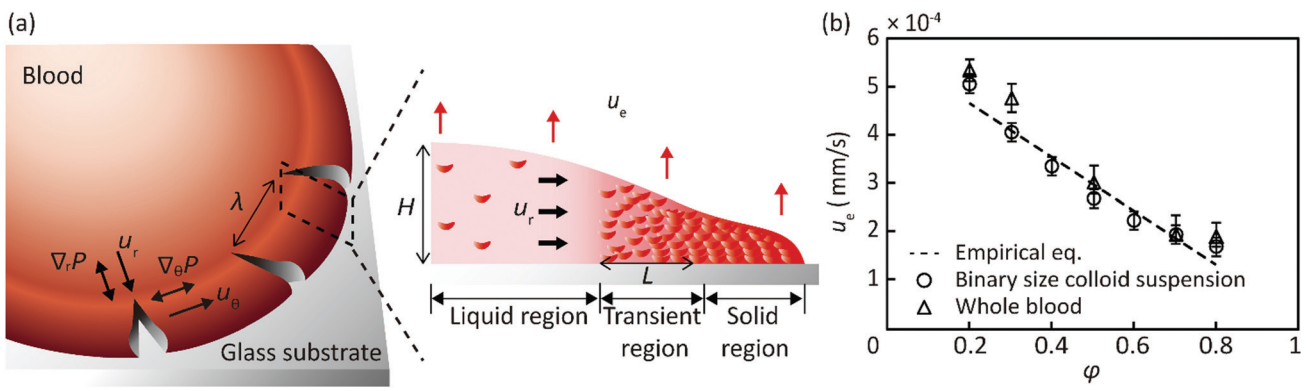

Fig. 2 Schematic illustrations of (a) bird's-eye and cross-sectional views of the cracks of a blood droplet. (b) Dependence of the evaporation rate of the whole blood and binary size colloid suspension on the relative humidity. The dashed line indicates the empirical model, $u_e = 6 \times 10^{-4}(1 - \phi)$ mm s^{-1}, obtained from the best linear fitting of the measured values. The error bars denote the maximum and minimum values in the multiple measurements.

model human blood as a colloid suspension mainly consisting of RBCs and albumin aggregations. We consider a particle cake between two adjacent cracks, as shown in Fig. 2a. Continuous water evaporation from the top surface causes local pressure drop owing to capillarity, and any non-uniform pressure distribution yields the plasma flow through the closely packed RBCs and albumin aggregation. Since the crack formation locally relieves the pressure non-uniformity,[14] the pressure near the crack recovers to the atmospheric pressure. A pressure gradient in the azimuthal direction normal to the crack, therefore, scales as $\nabla_\theta P \sim \sigma/(r\lambda)$, where $r \sim 10$ nm is the characteristic size of the albumin aggregation covering the porous structure, and λ is the inter-crack distance (see Fig. 2a). The plasma flow through the porous structure can be described by Darcy's law, so that the average flow speed in the direction normal to the crack is given by $u_\theta = -K\nabla_\theta P/\mu \sim K\sigma/(\mu r\lambda)$, where K is the permeability of the porous medium, and μ is the solvent viscosity. While K of a mono size (r) colloidal suspension is simply given by the Kozeny–Carman equation,[31,32] $K = 2r^2(1-\phi)^2/(75\phi^2)$ with ϕ the volume fraction of particles, K of a binary size suspension of large RBCs and small albumins depends on the sizes of both of the particle kinds. Here we adopt a model of mean radius of colloids,[33] $r_{av} = 2/[\phi_R/R + (1-\phi_R)/r]$ with R and ϕ_R, respectively, being the characteristic radius and volume ratio of RBCs and r the albumin radius, which leads to $K = 2r_{av}^2(1-\phi)^2/(75\phi^2)$ with ϕ being the volume fraction of RBCs and albumin.

A crack propagates from the drying edge to the central region of the droplet. Crack propagation speed is known to be proportional to the radial speed u_r of the plasma flow from the fluid region to the solidifying region (see Fig. 2).[15] Ignoring inertial effects, the radial flow in the thin droplet can be described by $\Delta_r P/L \sim \eta u_r/H^2$, where $\Delta_r P$ is the pressure difference across the solid–liquid transient region, L is the length scale of the transient region, η is the dispersion viscosity, and H is the liquid film thickness. The dispersion thickness varies in the transient region, and the interface curvature of the droplet film scales as H/L^2, so that $\Delta_r P \sim \sigma H/L^2$ *via* the Young–Laplace equation. The evaporation causes plasma flow in the vertical direction to the glass substrate,[34] and the continuity equation yields $u_r \sim (L/H)u_e$ with u_e being the rate of evaporation volume per unit area. As a result, we get $L/H \sim [\sigma/(\eta u_e)]^{1/4}$, and $u_r \sim (\sigma/\eta)^{1/4}u_e^{3/4}$. Because the azimuthal speed of the solvent u_θ is on the same order of magnitude as the radial speed u_r in the vicinity of the crack apex,[16,34] the scaling of $u_\theta \sim u_r$ leads to the expression for the crack density as $1/\lambda \sim \mu r u_e^{3/4}/(\eta^{1/4}\sigma^{3/4}K)$. Note that η may increase during the evaporation process, but it can be assumed to be constant because of the quarter power of η, which makes only small error.[16]

The evaporation rate u_e depends on the relative humidity ϕ. For a sessile water droplet, the evaporating mass is known to be proportional to $(1-\phi)$.[35] We measured the changes in the mass m of a 5 μl blood droplet and polystyrene colloidal dispersion on a 15 mm × 1 mm slide glass at 20 °C and at different relative humidity levels. Assuming $dm/dt = -\rho A u_e$ with t being time, the projection area of the droplet on the substrate A and the water density ρ, we found an empirical relation, $u_e = 6 \times 10^{-4}(1-\phi)$ mm s^{-1}, which holds for both the biological and artificial dispersions (see Fig. 2b). Then the crack density $f = 1/\lambda$ is given by:

$$f \sim \frac{\mu r(1-\phi)^{3/4}}{\eta^{1/4}\sigma^{3/4}K} \quad (1)$$

which reveals the physical parameters that determine the crack density.

We validate the model by examining the dependence of crack density on the solvent viscosity μ and the relative humidity ϕ using whole blood and colloidal dispersions of binary size polystyrene particles with diameters of 20 nm and 8 μm (Sigma-Aldrich). The zeta potential due to surface charge of the polystyrene particles is −20 mV,[36] which is similar to that of blood cells, approximately −14 mV.[37] The colloidal dispersions were sonicated at 40 kHz for 2 h. We controlled the volume ratio of the small to large particles to be approximately 0.1, comparable to the volume ratio of the albumin aggregation to RBCs. The volume ratio of the suspensions to liquid was set to be 0.5. We covered a 15 mm × 1 mm slide glass with a 5 μl droplet of blood or the polystyrene particle, and dried them in an environmental chamber (see Fig. 3a). Because the evaporation rate and solvent viscosity of blood depend on the temperature, we proceeded with the crack tests under a standard temperature condition (20 °C). The thickness of the droplet was measured to be approximately 0.3 mm for all cases. The droplet was pinned at the glass substrate edge, so that the contact angle did not affect our experimental results.[12] As shown in Fig. 3b, the cracks were

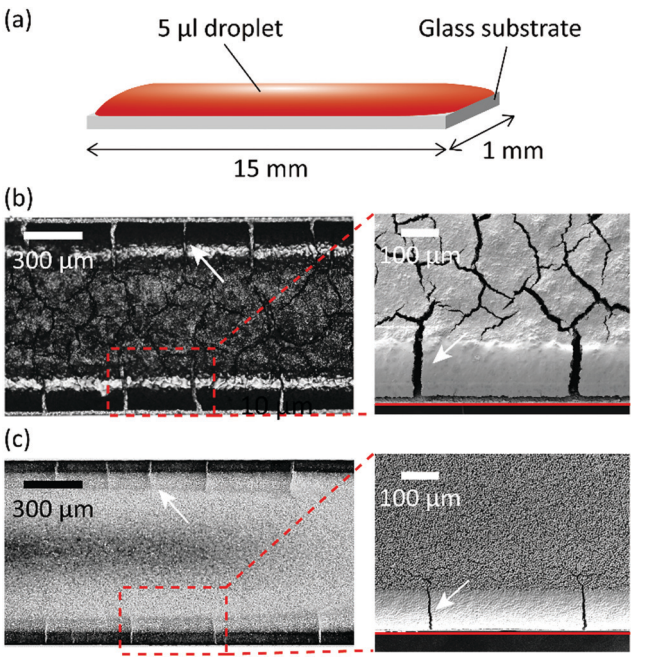

Fig. 3 Drying experiments of whole blood and colloidal dispersion droplets. (a) The sample droplet deposited on a glass substrate of 15 mm × 1 mm. Optical (left) and SEM (right) images of cracks of (b) blood and (c) the binary size colloid dispersion on the glass substrate edge. The red solid lines and white arrows indicate the substrate edge and the cracks, respectively.

formed mostly in the direction orthogonal to the glass edges in both cases, which facilitated the quantification of the crack density. We estimated the crack density f by measuring the number of cracks for the edges with a length of approximately 22 mm in each sample.

Fig. 4 presents the effects of the environmental humidity and the blood viscosity on the crack density. In Fig. 4a, the crack density decreases with the relative humidity, showing good agreement with the model prediction indicated by the solid line. Fig. 4b shows the effects of the viscosity on the crack density. Noting that the blood viscosity, approximately 4 mPa s in the normal condition, can be as large as 10 mPa s for persons with diabetes due to glucose content, we varied the suspension viscosity by adding glucose to the normal whole blood and the polystyrene dispersion. The results show that the crack density increases with viscosity, and a viscosity change of 10 mPa s results in approximately 25% increase in the blood crack density, as predicted by eqn (1).

In the insets of Fig. 4a and b, we included the crack density data of mono size colloid suspensions containing 20 nm particles. We found that the mono size dispersion also generates cracks, whose density increases with increase of viscosity and decrease of relative humidity. However, the crack density of the mono size colloid dispersion is much higher than that of the binary size

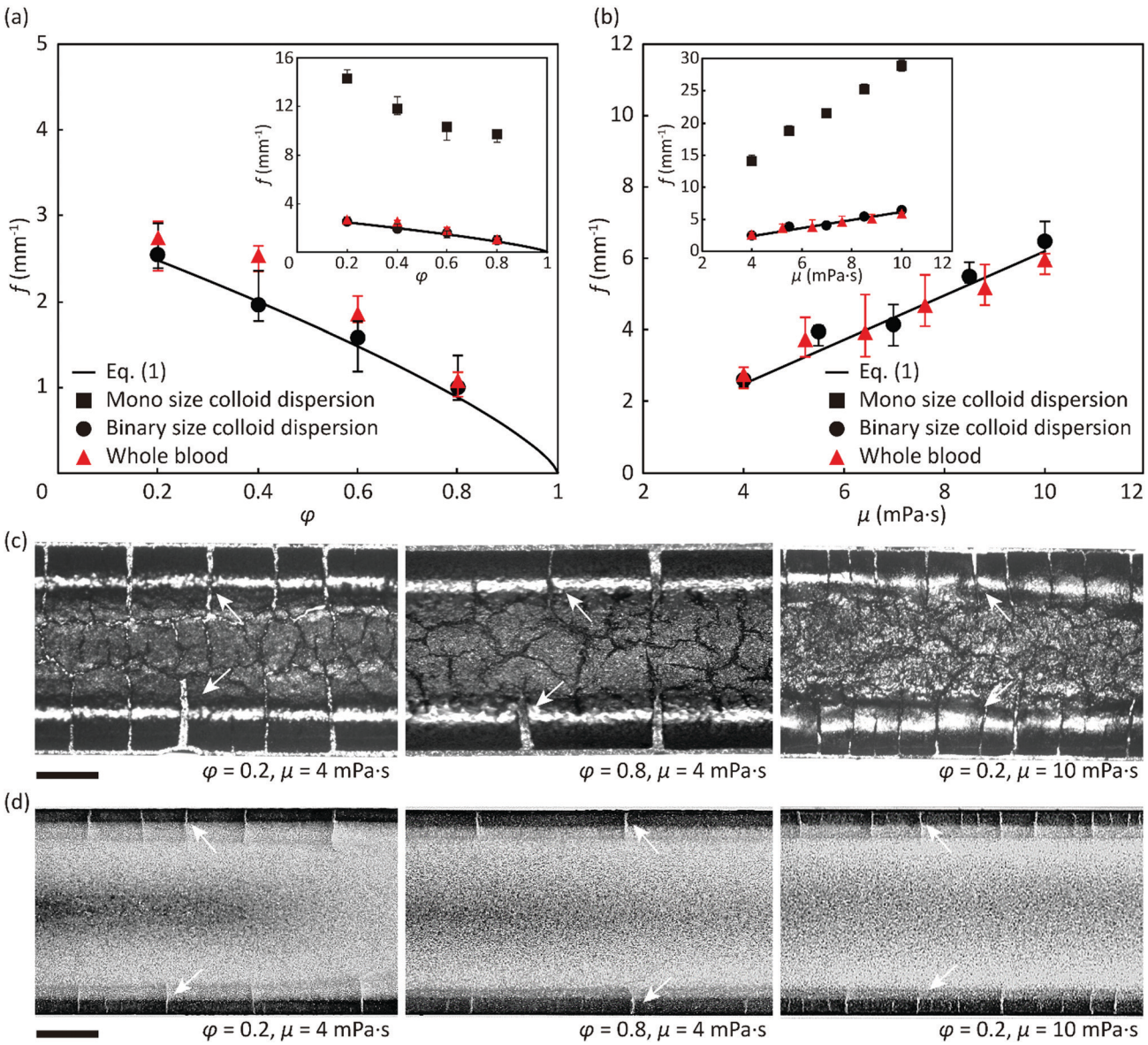

Fig. 4 Measurement and visualization of the crack density on relative humidity and blood viscosity. Crack density (a) decreases with the relative humidity and (b) increases with the blood viscosity. The humidity and viscosity were fixed at 4 mPa s and 20%, respectively, when these were not changed. The insets include the crack density of the mono size colloid dispersion containing 20 nm particles. The error bars denote the maximum and minimum values in the multiple measurement (n = 3 or 4). Optical images showing the cracks of (c) the bloodstains and (d) the binary size colloid dispersion. The white arrows indicate the cracks. Scale bars, 300 μm.

colloid dispersion, clearly indicating the importance of considering binary size distribution of colloid particles in analysing human bloodstain cracks.

As we have verified that the cracks of bloodstains can be understood based on the binary size colloid assumption, it is possible to investigate the role of particles of each size in crack formation. Fig. 5a and b compare the dried stains of mono size colloid suspensions of 8 μm (a) and 20 nm (b) polystyrene particles. We see that suspensions containing only 8 μm particles fail to exhibit cracks when dry, while suspensions of 20 nm particles generate cracks. Thus, we find that RBCs alone cannot induce cracks, while proteins are a main factor of blood cracking. But the crack density is modulated by RBCs as the permeability K depends on the radius and volume ratio of RBCs.

To further verify the role of RBCs and proteins in crack formation, we created a binary size colloid dispersion with an increased volume ratio of small to large particles, 0.26, so that most of the pores between large particles are filled with smaller particles. The experimental results displayed in Fig. 5c reveal lower crack density (greater spacings between cracks) in the binary size colloid dispersion than in the mono size colloid dispersion of Fig. 5b. This distinction can be explained based on the permeability K from eqn (1), where K is proportional to the square of particle diameter.[16,33] As the mean diameter of the binary size colloid dispersion is larger than that of the mono size colloid dispersion, we can deduce that $K_{binary}/K_{mono} > 1$, which means $f_{binary}/f_{mono} < 1$. Therefore, we can anticipate that the large particles hinder the crack formation, which is caused mainly by small particles, allowing us to envision the role of the large blood cells and small proteins in the crack density.

Although our model successfully predicts the crack density in normal blood, the crack patterns in bloodstains with diseases, such as anemia, hyperlipidemia, jaundice, and thalassemia, are known to differ from that of bloods obtained from healthy people in terms of the direction and thickness of cracking.[3,4] Since it is still unclear how the biological properties of blood affect crack density, in future work it will be valuable to examine the crack density of bloods with various biological properties.

In summary, we have proposed a theoretical model to understand the crack density in a bloodstain. The visualization of cracks formed on the dried blood droplet has allowed us to model blood as a binary size colloid suspension. Building upon the classical theory of crack formation in a colloid suspension, we have suggested a mathematical model for the crack density of bloodstains, which has been validated by experiments using the binary size colloid suspension and the whole blood. The model has revealed the effects of the relative humidity and the

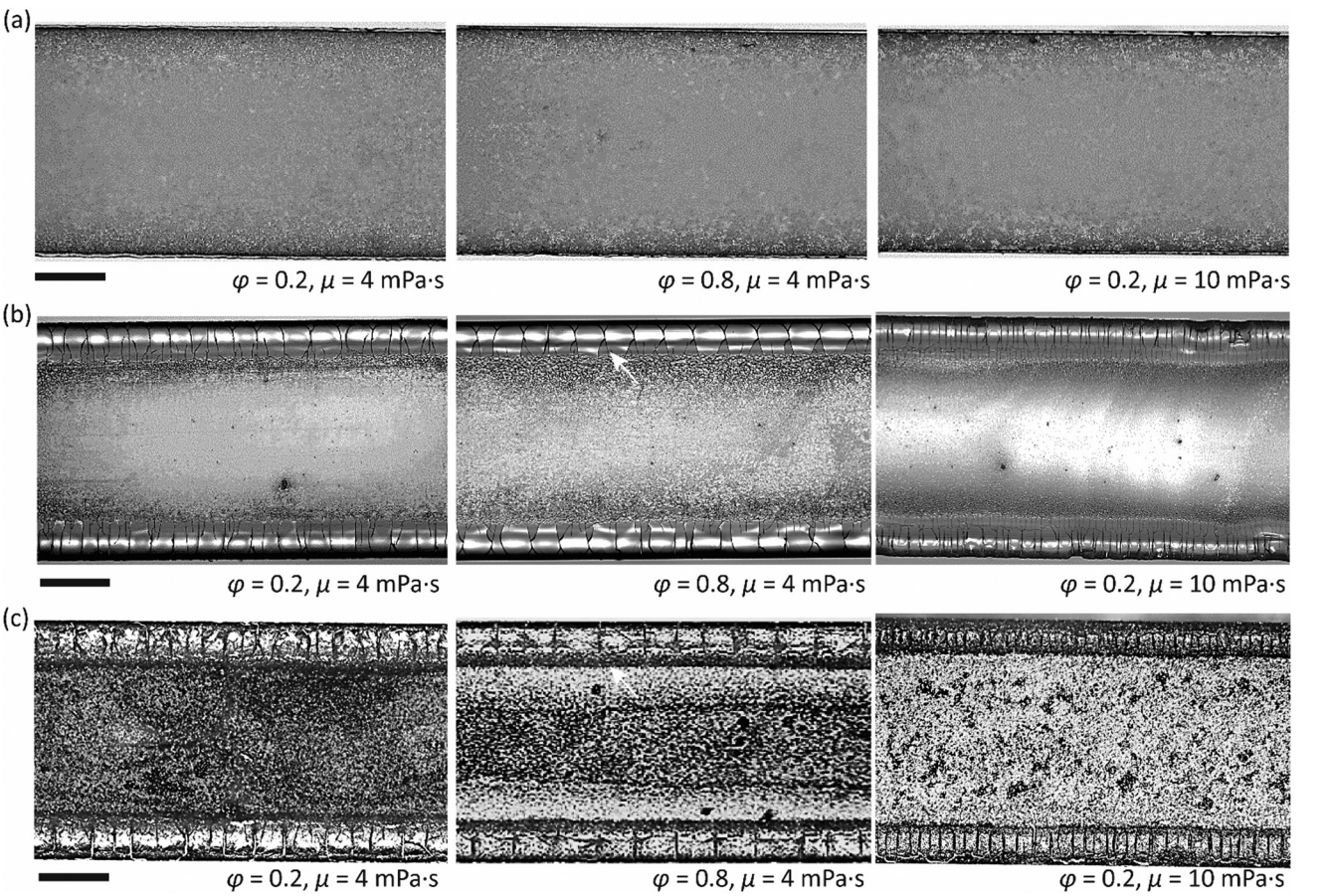

Fig. 5 Optical images showing the cracks of (a) 8 μm and (b) 20 nm mono dispersion and (c) the binary size colloid dispersion. The volume ratios of suspensions to liquid are comparable to those of blood constituents. The white arrows indicate the cracks. Scale bars, 300 μm.

viscosity on the crack density. Given that blood viscosity changes sensitively for patients with diabetes, AIDS, and atherosclerosis,[38–40] our results can provide insight into developing techniques for disease diagnosis. Furthermore, the humidity of the dehydration environment inferred from blood cracks can serve as useful forensic information.

Conflicts of interest

There are no conflicts to declare.

Acknowledgements

This work was supported by the National Research Foundation of Korea (grant no. 2018052541 and 2017R1E1A1A01073599) and administered *via* SNU IAMD.

Notes and references

1 J. Gao, L. Li, P.-L. Ho, G. C. Mak, H. Gu and B. Xu, *Adv. Mater.*, 2006, **18**, 3145–3148.
2 Z. Huang, A. Gallot, N. T. Lao, S. J. Puechmaille, N. M. Foley, D. Jebb, M. Bekaert and E. C. Teeling, *Mol. Ecol. Resour.*, 2016, **16**, 150–162.
3 D. Brutin, B. Sobac, B. Loquet and J. Sampol, *J. Fluid Mech.*, 2011, **667**, 85–95.
4 L. Bahmani, M. Neysari and M. Maleki, *Colloids Surf., A*, 2017, **513**, 66–75.
5 W. B. Zeid and D. Brutin, *Colloids Surf., A*, 2013, **430**, 1–7.
6 W. B. Zeid, J. Vicente and D. Brutin, *Colloids Surf., A*, 2013, **22**, 139–146.
7 D. Brutin, B. Sobac and C. Nicloux, *J. Heat Transfer*, 2012, **134**, 061101.
8 N. Laan, F. Smith, C. Nicloux and D. Brutin, *Forensic Sci. Int.*, 2016, **267**, 104–109.
9 R. Chen, L. Zhang, D. Zang and W. Shen, *J. Mater. Chem. B*, 2017, **45**, 8991–8998.
10 W. Choi, J. Shin, K.-A. Hyun, J. Song and H.-I. Jung, *Biosens. Bioelectron.*, 2019, **130**, 414–419.
11 S. Shiri, K. F. Martin and J. C. Bird, *Forensic Sci. Int.*, 2019, **295**, 189–198.
12 R. Chen, L. Zhang and W. Shen, *J. Mater. Chem. B*, 2018, **6**, 5867–5875.
13 B. Sobac and D. Brutin, *Colloids Surf., A*, 2014, **448**, 34–44.
14 C. Allian and L. Limat, *Phys. Rev. Lett.*, 1995, **74**, 2981–2984.
15 E. R. Dufresne, E. I. Corwin, N. A. Greenblatt, J. Ashmore, D. Y. Wang, A. D. Dinsmore, J. X. Cheng, X. S. Xie, J. W. Hutchinson and D. A. Weitz, *Phys. Rev. Lett.*, 2003, **91**, 224501.
16 W. P. Lee and A. F. Routh, *Langmuir*, 2004, **20**, 9885–9888.
17 M. S. Tirumkudulu and W. B. Russel, *Langmuir*, 2005, **21**, 4938–4948.
18 K. B. Singh and M. S. Tirumkudulu, *Phys. Rev. Lett.*, 2007, **98**, 218302.
19 M. Leang, F. G. Dauphine, L. T. Lee and L. Pauchard, *Soft Matter*, 2017, **13**, 5802–5808.
20 H. P. Erickson, *Biol. Proced. Online*, 2009, **11**, 32–51.
21 R. Murray, P. A. Mayes, V. W. Rodwell and D. K. Granner, *Harper's Biochemistry, Appleton & Lange*, 25th edn, 2000.
22 M. L. Ferrer, R. Duchowicz, B. Carrasco, J. G. Torre and A. U. Acuna, *Biophys. J.*, 2001, **80**, 2422–2430.
23 W. J. Marshall and S. K. Bangert, *Clinical Chemistry*, Elsevier, 6th edn, 2008.
24 M. Lieberman and A. Marks, *MARKS' Basic Medical Biochemistry*, Lippincott Williams & Wilkins, 4th edn, 2012.
25 R. D. Deegan, O. Bakajin, T. F. Dupont, G. Huber, S. R. Nagel and T. A. Witten, *Nature*, 1997, **389**, 827–829.
26 A. F. Routh, *Rep. Prog. Phys.*, 2013, **76**, 046603.
27 G. L. Brown, *J. Polym. Sci.*, 1956, **22**, 423–434.
28 D. P. Sheetz, *J. Appl. Polym. Sci.*, 1965, **9**, 3759–3773.
29 P. Xu, A. S. Mujumdar and B. Yu, *Drying Technol.*, 2009, **27**, 636–652.
30 J. Ha and H.-Y. Kim, *Annu. Rev. Fluid Mech.*, 2020, **52**, 263–284.
31 J. Kozeny, *Stizungsber. Akad. Wiss. Wien*, 1927, **16**, 271–306.
32 P. C. Carman, *Trans. Inst. Chem. Eng.*, 1937, **15**, 150–156.
33 M. Mota, J. A. Teixeria, W. R. Bowen and A. Yelshin, *Trans. Filtr. Soc.*, 2001, **1**, 101–106.
34 W. P. Lee and A. F. Routh, *Ind. Eng. Chem. Res.*, 2006, **45**, 6996–7001.
35 H. Hu and R. G. Larson, *J. Phys. Chem. B*, 2002, **106**, 1334–1344.
36 H. Sun and N. Hu, *Biophys. Chem.*, 2004, **110**, 297–308.
37 H. P. Fernandes, C. L. Cesar and M. L. B. Castro, *Rev. Bras. Hematol. Hemoter.*, 2011, **33**, 297–301.
38 L. Dintenfass, *Vasc. Surg.*, 1980, **14**, 227–237.
39 G. D. O. Lowe, *Ann. Peridontol.*, 1998, **3**, 121–126.
40 A. M. Robertson, A. Sequeira and M. V. Kameneva, *Hemorheology in Hemodynamical Flows: Modeling, Analysis and Simulation*, Oberwolfach Seminars Series, Birkhauser, Boston, 2008.

